DMD Fast Forward. Published on March 9, 2018 as DOI: 10.1124/dmd.117.079442
This article has not been copyedited and formatted. The final version may differ from this version.

Title page

A Promising Microtubule Inhibitor Deoxypodophyllotoxin Exhibits Better Efficacy to Multi-Drug Resistant Breast Cancer than Paclitaxel via Avoiding Efflux Transport

Xiaojie Zang, Guangji Wang, Qingyun Cai, Xiao Zheng, Jingwei Zhang, Qianying Chen, Baojin Wu, Xiong Zhu, Haiping Hao and Fang Zhou

Key Laboratory of Drug Metabolism and Pharmacokinetics, State Key Laboratory of Natural Medicines, China Pharmaceutical University, Nanjing, China (X.Z., G.W., Q.C., X.Z., J.Z., Q.C., H.H., F.Z.)

Medical and Chemical Institute, China Pharmaceutical University, Nanjing, China (B.W., X.Zhu.)

DMD Fast Forward. Published on March 9, 2018 as DOI: 10.1124/dmd.117.079442
This article has not been copyedited and formatted. The final version may differ from this version.

Running Title page

A Promising Microtubule Inhibitor Overcomes MDR

*Corresponding author: Fang Zhou

Key Laboratory of Drug Metabolism and Pharmacokinetics, State Key Laboratory of Natural Medicines, China Pharmaceutical University, Nanjing, China

E-mail: zf1113@163.com

Co-corresponding author: Haiping Hao,

State Key Laboratory of Natural Medicines, China Pharmaceutical University, Nanjing, China

Tel.: +86 25 83271060; Fax: +86 25 83271060.

E-mail: hhp_770505@hotmail.com

Number of Text pages: 42

Number of Tables: 1

Number of figures: 7

Number of references: 41

Number of words in Abstract: 240

Number of words in Introduction: 720

Number of words in Discussion: 1164

Abbreviations

ANOVA, One-way analysis of variance; AUC, area under the curve; BCRP, Breast Cancer Resistance Protein; DOX, Digoxin; DPT, deoxypodophyllotoxin; ER, efflux ratio; ESI,

DMD Fast Forward. Published on March 9, 2018 as DOI: 10.1124/dmd.117.079442
This article has not been copyedited and formatted. The final version may differ from this version.

electrospray ionization; MCF-7/A, MCF-7/Adr; MDCK, Madin–Darby canine kidney epithelial cells; MDR**,** multi-drug resistance; MRP2, Multi-drug Resistance-associated Protein 2; P_{app}, apparent permeability values; P-gp, P-glycoprotein; PTX, paclitaxel.

DMD Fast Forward. Published on March 9, 2018 as DOI: 10.1124/dmd.117.079442
This article has not been copyedited and formatted. The final version may differ from this version.

Abstract

Multi-drug resistance (MDR) is a common limitation for the clinical use of microtubule-targeting chemotherapeutic agents and it is the main factor for poor prognoses in cancer therapy. Here, we report on deoxypodophyllotoxin (DPT), a promising microtubule inhibitor in phase I, as a promising candidate to circumvent the obstacle. DPT remarkably suppressed the tumor growth in xenograft mice bearing either Paclitaxel (PTX)-sensitive MCF-7/S or acquired resistance MCF-7/Adr (MCF-7/A) cells. Also, DPT exhibited a similar accumulation in both tumors, while PTX displayed much a lower accumulation in the resistant tumors. *In vitro*, DPT exhibited a much lower resistance index (0.552) than those of PTX (754.5) or Etoposide (38.94) in both MCF-7/S and MCF-7/A cells. Flow cytometry analysis revealed that DPT (5, and 10 nM) caused the arrest of the G2/M phase in the two cell lines, while PTX (up to 10 nM) had no effect on the cell cycle progression of the MCF-7/A cells. Microtubule dynamics assays revealed that DPT destabilized microtubule assembly in a different mode. Cellular pharmacokinetic assays indicated comparable intracellular and subcellular accumulations of DPT in the two cell lines but a much lower retention of PTX in the MCF-7/A cells. Additionally, transport assays revealed that DPT was not the substrate of P-glycoprotein (P-gp), Breast Cancer Resistance Protein (BCRP), or Multi-drug Resistance-associated Protein 2 (MRP2), indicating a lower occurrence rate of multi-drug resistance. DPT might be a promising microtubule inhibitor for breast cancer therapy, especially for treatment of drug-resistant tumors.

DMD Fast Forward. Published on March 9, 2018 as DOI: 10.1124/dmd.117.079442
This article has not been copyedited and formatted. The final version may differ from this version.

1. Introduction

Microtubules are mainly composed of α- and β-tubulin heterodimers, which can be bounded by two groups: microtubule-stabilizing agents and microtubule-destabilizing agents. As reported, microtubule-bindings agents are involved in numerous fundamental intracellular processes, such as the most recognized, mitosis (Howard and Hyman, 2003), thus they receive a great deal of attention in the treatment of cancer. Anti-microtubule drugs are one type of the most effective drugs in the treatment of breast cancer, ovarian cancer, and other tumors. However, the occurrence of multi-drug resistance (MDR) is a common limitation in their clinical use. Paclitaxel (PTX), a microtubule-stabilizing agent that has been approved by the Food and Drug Administration for breast and lung cancer treatment, has demonstrated to be the P-glycoprotein (P-gp) efflux pump substrate that causes increased efflux (Gottesman, 1993) and consequently reduces Paclitaxel's intracellular concentration and develops drug resistance to the breast cancer therapy (Dumontet and Jordan, 2010). Therefore, novel microtubule inhibitors with high efficacy to multi-drug resistant tumors are greatly needed.

Deoxypodophyllotoxin (DPT), isolated from *Anthriscus sylvestris,* is an active component that has potent anti-proliferative and anti-tumor effects against a broad variety of cancer types by modulating the microtubule (Shin et al., 2010; Khaled et al., 2013; Kim et al., 2013; Wang et al., 2015b; Khaled et al., 2016). As the promising microtubule inhibitor, DPT and its intravenous formulation of β-cyclodextrin inclusion complex (Zhu et al., 2010) have been adopted for phase I evaluation. A physiologically based pharmacokinetics model was also established for better efficacy and safety assessment (Chen et al., 2016). Previous studies have demonstrated that DPT exerts an anti-tumor effect on the human BC MDA-MB-231 cell

line *in vivo* and *in vitro* (Benzina et al., 2015; Khaled et al., 2016). However, the effect of DPT on drug-resistant cancer cells has yet to be investigated. Whether DPT treatment can induce drug efflux transporters and subsequently lead to multi-drug resistance warrants further confirmation.

From macrocosm to microcosm, intracellular pharmacokinetics has attracted great attention to the monitoring of intracellular target binding and the intracellular disposition process of drugs (Tulkens, 1990; Krishan et al., 1997), including drug uptake, distribution, metabolism, and efflux within the cellular environment. In recent studies, Adriamycin resistance in MCF-7/A cells was identified by exploring the cellular pharmacokinetic mechanism, which could be reversed by inhibiting P-gp (Zhang et al., 2012). Therefore, intracellular pharmacokinetics has provided a new perspective (Zhou et al., 2011) to determine the underlying mechanisms of MDR, thus promoting efficacy in drug discovery to overcome MDR.

In the current study, we aimed to investigate the anti-tumor effect of DPT on both drug-sensitive and drug-resistant MCF-7 cell lines *in vivo* and *in vitro*. We also explored the discrepancy between PTX and DPT on MDR from the perspective of intracellular pharmacokinetics. In parallel, the potential of DPT to overcome MDR was further disclosed.

2. Materials and Methods

2.1 Reagents

DPT (purity > 99%) and DPT-HP-β-CD (content: 2.8%) were kindly provided by the Medicinal and Chemical Institute, China Pharmaceutical University (Chen et al., 2016).

Paclitaxel (injection) was purchased from the Yangtze River Pharmaceutical Group (Jiangsu, China). Etoposide, Digoxin, PTX, and Verapamil were bought from Sigma-Aldrich (St. Louis, USA). Lovastatin was obtained from the Chinese National Institute for the Control of Pharmaceutical and Biological Products (Beijing, China). Acetonitrile and methanol (Merck, Germany) were of HPLC grade. Acetic acid and ammonium acetate of HPLC grade were purchased from Adamas Reagent Co., Ltd (Shanghai, China). Analytical-grade sodium acetate was from Nanjing Chemical Reagent Co., Ltd (Jiangsu, China).

2.2 Animals

Female athymic BALB/c nude mice (9 weeks old, 18-22 g) were purchased from Shanghai Slack Laboratory Animal Co., Ltd. (Shanghai, China). The mice received 5×10^6 exponentially growing MCF-7/S and MCF-7/A cells subcutaneously on the right flank and estrogen pellets were implanted before injection. Before the experiment, the mice were housed 10 per cage in a constant temperature and humidity with an automatic day-night rhythm (12 h-cycle) in a SPF-grade environment. When the tumors reached 100 mm^3, the mice were randomly divided into three groups, following by subjection to antitumor treatment. Prior to the experiment, the mice fasted overnight (12 h) with free access to water. The Guidelines for Care and Use of Laboratory Animals and the protocols approved by the corresponding Animal Ethics Committee of China Pharmaceutical University (Nanjing, China) were followed throughout all of the animal experiments.

2.3 Anti-tumor activity of DPT and PTX in tumor xenograft models

Mice bearing MCF-7/S and MCF-7/A subcutaneous tumors in their right flank regions were randomly assigned to three groups (10 and 9 mice per group, respectively): (a) control

group (saline, i.v.); (b) DPT (12.5 mg/kg, i.v.); and (c) PTX (12.5 mg/kg, i.v.). Mice in each group were administrated once every three days and weighed, and the major (a) and minor (b) axes of tumors were monitored daily. The tumor volume was calculated according to the formula: TV (mm^3) = 1/2 × a × b^2. The survival ratio of the two models was over 75%, so at least 6 mice in each group were guaranteed to be alive 10 days later. After 10 days, the mice were killed by CO_2 asphyxiation, and the plasma, xenografts, heart, liver, spleen, lung, and kidney were collected. The rate of tumor volume growth was calculated using the following formula:

Reduction rate = (1- mean of treatment group/mean of control group) × 100%.

2.4 Cell culture

Human breast cancer cells MCF-7 (MCF-7/S), which were purchase from the American Type Culture Collection (Rockville, MD, USA), and their acquired resistant cells (MCF-7/A; by long-termed doxorubicin induction) were provided by the Institute of Hematology and Blood Diseases Hospital (Tianjin, China). MCF-7/A cells have been verified to overexpress P-gp compared to MCF-7/S cells and they exhibit multi-drug resistance (Zhang et al., 2012). These two cell lines were cultured in RPMI 1640 supplemented with 10% fetal bovine serum and 100 $U \cdot mL^{-1}$ penicillin and streptomycin (Invitrogen, Carlsbad, CA, USA) at 37°C with 5% CO_2. $CaCO_2$ cells, parent Madin–Darby canine kidney epithelial cells (MDCK), and MDR1-transfected MDCK cells (MDR1-MDCK) were obtained from ZheJiang University (Hangzhou, China) (Cao et al., 2011). Cells were cultured in Dulbecco's modified Eagle's medium, along with 10% fetal bovine serum, and 100 $U \cdot mL^{-1}$ penicillin and streptomycin.

2.5 Cytotoxicity assay

The efficacy of PTX and DPT on MCF-7/S and Adriamycin-resistant MCF-7/A cells was determined by cell growth inhibition via 3-(4,5-dimethyl-2-thiazolyl)-2,5-diphenyl-2Htetrazolium bromide colorimetric assay after incubation with PTX and DPT under different concentrations. The concentration required to inhibit growth by 50% (IC_{50} values) were calculated from the survival curves using the Bliss method (Bliss, 1939, Zhang et al., 2012; Lu et al., 2015).

2.6 Cell cycle analysis

Cell cycle distribution was addressed by determining the DNA content of the cells. Cells were fixed at 4°C in ethanol overnight and then re-suspended in staining solutions containing RNase A (100 μg/mL) and propidium iodide (20 μg/mL) for 30 min. Finally, the DNA content was monitored by flow cytometry (FACS Calibur, BD, Franklin Lakes, New Jersey, USA) and analyzed with CELLQUEST software (Becton-Dickinson, San Jose, CA, USA).

2.7 Cellular retention assay

The cells from passages 10-20 were seeded on 24-well cell culture plates. When 90% confluency was reached, the cells were treated with DPT or PTX (5 μM) for 15, 30, 60, and 120 min. After 2 h of incubation, the cells were lysed via 3 freeze-thaw cycles. As for the efflux assay, the cells were incubated with DPT or PTX (5 μM) for 2 h, then the intracellular retention of the two drugs with or without Verapamil (20 μM) was determined after 0, 15, 30, 60 and 120 min. Meanwhile, the protein concentrations were measured by the Bradford method (Bradford, 1976). The concentration of DPT was determined by LC-MS/MS, and PTX was monitored as previously described (Liu et al., 2017). All of the experiments were conducted in triplicate. The AUC of the intracellular accumulation was expressed with the

DMD Fast Forward. Published on March 9, 2018 as DOI: 10.1124/dmd.117.079442
This article has not been copyedited and formatted. The final version may differ from this version.

average concentration of DPT or PTX after 2 h of incubation.

2.8 Subcellular distribution of DPT and PTX

MCF-7 cells from passages 10-20 were cultured in 75 cm^2 cell culture flasks. Upon reaching 90% confluency (over 10^7 cells/flask), the cells were treated with PTX or DPT (1 μM). After 15, 30, 45 min, 1, 2 h of incubation, the cytoplasm, mitochondria, and nuclei were extracted according to the instructions of the KeyGen Mitochondria/Nuclei Isolation Kit (Nanjing KeyGen Biotech. Co., Ltd., China) as we described previously (Zhang et al., 2012) . Meanwhile, the protein content of the cytoplasm, mitochondria, and nuclei was determined as described above. Then, the concentration of DPT and PTX in each subcellular compartment was measured by LC-MS/MS, and it was further adjusted in terms of the original dosing volume. The AUC of the subcellular accumulation was expressed with the average concentration of DPT or PTX after incubation for 2 h.

2.9 Tubulin polymerization assay

The experiment was performed according to a Tubulin Polymerization Assay Kit (Cytoskeleton, Denver, CO, USA). Briefly, the standard polymerization reaction containing 3 mg/mL tubulin in G-PEM (80 mM PIPES,0.5 mM EGTA, 2 mM $MgCl_2$, 1mM GTP, and 10% glycerol, PH 6.9) was mixed with different compounds in a 96-well plate. Polymerization was started by incubation at 37°C and followed by absorbance readings at 340 nm every minute for 1 h. All of the experiments were repeated three times.

2.10 Transport assays

Parent and MDR1-transfected Madin–Darby canine kidney epithelial cells from passages 10-20 were seeded at 5×10^5 cells per 1.12 cm^2 density on Millipore Millicell inserts

DMD Fast Forward. Published on March 9, 2018 as DOI: 10.1124/dmd.117.079442
This article has not been copyedited and formatted. The final version may differ from this version.

(Millipore Corporation, Bedford, MA, USA; 12 mm in diameter, 0.4 μm pore size) in 24-well tissue culture plates. Transport studies were conducted 5 days after seeding. Briefly, the MDCK and MDR1-MDCK cells were gently rinsed with HBSS followed by incubation for 20 min at 37°C. To evaluate the effect of P-gp inhibitor on the transport of DPT, Verapamil (20 μM) was added to either the apical or basolateral side of the monolayer 30 min prior to the addition of DPT (0.5 and 1 μM) or digoxin (5 μM) for 2 h. The apparent permeability values (P_{app}) were calculated according to the following formula (Ranaldi et al., 1996; Zhang et al., 2010; Poirier et al., 2014; Kodama et al., 2016):

$$P_{app} = \frac{dQ/dt}{AC_0},$$

where dQ/dt represents the slope of the transporter cumulative amount within the time course studied, A is the surface area of the Millicell inserts, and C_0 is the initial concentration. The efflux ratio (ER) was obtained by calculating the ratio of $P_{app\ B\text{-}A}$ to $P_{app\ A\text{-}B}$. A compound with a ratio larger than 2.0 was qualified as a substrate of the efflux mechanism.

2.11 Histopathological examination

Tumor tissues were collected and processed for histopathological examination. Briefly, tumors were fixed in 4% paraformaldehyde and then embedded in paraffin wax. Sections were subsequently prepared at a thickness of 4 μm and stained with hematoxylin and eosin. The percentage of the lesion area was calculated according to 5 random images from the sections of the individual mice captured by light microscope (Zeiss, Germany).

2.12 LC-MS/MS method for DPT quantification

Briefly, a 50-μL aliquot of the cell sample was precipitated with 150 μL acetonitrile (containing lovastatin as the internal standard). After centrifugation, 10 μL of the supernatant

was injected into the SCIEX 5500 system (Framingham, MA, USA) with a Waters C18 column (3.0× 50 mm, 2.5 μm, Waters, Milford, MA, USA). The column and autosampler tray temperatures were designated as 40 and 4°C, respectively. Mobile phase A used 0.1% (v/v) acetic acid and 2 mM ammonium acetate in water, and mobile phase B used acetonitrile. A gradient 0 min; 30% B → 2 min; 70% B → 4 min; 70% B → 6 min; 30% B → 7 min; 30% B → 8 min. The flow rate was 0.2 mL/min. The mass spectrometer was operated in the positive electrospray ionization (ESI) mode. MS parameters were set as: Ion Source Gas 1 as 55, Ion Source Gas 2 as 35; Curtain gas as 15; Collision Gas as Medium, Temperature 550°C; and Ionspray Voltage: 5.5 kV in the positive mode. Quantification was performed using the selected reaction monitoring mode: m/z 399.2→157 with Declustering potential 85 V and collision energy 35 V for DPT; m/z 405 → 199 with DP 75 V and CE 36 V for lovastatin. To ensure reliability, we evaluated the method via linearity, recovery and matric effect, precision and accuracy, and stability validation, which were in line with the bioanalytical recommendations (supplementary data). The concentration of DPT in mice plasma and tissues were monitored as previously described (Yang et al., 2012) with quality control involved.

2.13 Statistical analysis

All of the data are presented as mean ± S.D. Significance was determined between two groups using the Student's *t* test. Multiple comparisons were analyzed with one-way analysis of variance (ANOVA). Representative graphs were made using GraphPad Prism 6.0 (GraphPad Software Inc., CA, USA) and p values <0.05 were considered to be statistically significant.

DMD Fast Forward. Published on March 9, 2018 as DOI: 10.1124/dmd.117.079442
This article has not been copyedited and formatted. The final version may differ from this version.

3. Results

3.1 DPT inhibited the tumor growth of both MCF-7/S and MCF-7/A xenograft mice *in vivo*

We first established two xenograft models of drug-sensitive and drug-resistant human breast cancer (MCF-7/S and MCF-7/A, respectively) to investigate the toxic effect of DPT *in vivo*. DPT was intravenously (12.5 mg/kg) administered every three days. Concomitantly, the comparison was conducted with the same dose of PTX every three days. Ten days after the last administration, as shown in Fig. 1A and 1E, both DPT and PTX exerted remarkable suppression of MCF-7/S xenograft growth. The average tumor weight of the MCF-7/S xenografts treated with DPT and PTX was 0.26 g and 0.28 g, respectively, compared with that of the vehicle-treated animals of 0.56 g (Fig. 1C). Fig. 1G revealed the inhibition of tumor volume growth of the MCF-7/S xenografts when supplemented with DPT (49.62%), while PTX caused the inhibition of tumor volume growth of 53.86%.

As displayed in Fig. 1B and 1F, DPT also showed a palpable reduction of the tumor growth of the MCF-7/A model, with the tumor weight of 0.17 g in contrast with that of the control group of 0.24 g (Fig. 1D). It was noteworthy that PTX showed just a marginal inhibitory rate (Fig. 1H), with the tumor weight of 0.24 g.

Additionally, no obvious body weight loss or abnormal behavior was observed in all of the DPT-treated groups. However, we found a distinguished loss of body weight in the PTX-treated MCF-7/A xenograft models. All of the results demonstrated that DPT was effective in the treatment of both sensitive and drug-resistant human breast cancer and showed no obvious toxicity. Conversely, PTX exerted a low tumor inhibition rate, suggesting that

DMD Fast Forward. Published on March 9, 2018 as DOI: 10.1124/dmd.117.079442
This article has not been copyedited and formatted. The final version may differ from this version.

PTX might develop resistance to the MCF-7/A cell lines.

3.2 DPT induced tumor necrosis in both the MCF-7/S and MCF-7/A xenografts

Histopathological examination of the xenografts was also performed in the MCF-7/S and MCF-7/A xenograft models. As shown in Fig. 2A and 2B, the tumor cells grew vigorously and arranged irregularly with more chromatin in the control group. However, under the treatment of DPT, the lesion areas of the MCF-7/S and MCF-7/A xenografts were 68%±7% and 25%±12%, respectively, within which, the sparsely arranged tumor cells were diffusely distributed with a pale cytoplasm, polymorphous nuclei and necrosis and mitotic activity was absent. In sharp contrast to DPT, PTX exerted no effects on the MCF-7/A xenografts.

3.3 DPT displayed comparable biodistribution in the MCF-7/S and MCF-7/A xenograft models

In support of the notion that DPT was more effective in the treatment of MCF-7/A xenografts, we next monitored the biodistribution of DPT and PTX in both the MCF-7/S and MCF-7/A xenograft models. The drug concentrations in the plasma were determined at 5 min and 45 min after DPT and PTX administration (Fig. 3A). Subsequently, the concentrations of DPT and PTX in the xenografts were monitored at 45 min. As presented in Fig. 3B, the concentration of DPT in the MCF-7/A xenografts was a little higher than that in the MCF-7/S xenografts, along with a parallel plasma/tumor ratio (Fig. 3C). Conversely, in contrast with the MCF-7/S xenografts, the concentration of PTX was decreased by 4.26-fold in the MCF-7/A xenografts, and the plasma/tumor ratio was decreased by 2.15-fold. Meanwhile, PTX was distributed less in other non-malignant tissues (Fig. 3D).

3.4 DPT exhibited a much lower resistance index than that of PTX or Etoposide in the

MCF-7/S and MCF-7/A cells

Based on the findings above, we next investigated the toxic effect of DPT on breast cancer cells. We chose MCF-7/S and their derivative MCF-7/A cells treated with different drugs at various concentrations to measure the cellular viabilities. As shown in Table 2, the IC_{50} values of DPT on the MCF-7/S and MCF-7/A cells were 10.61 nM and 5.86 nM, respectively, which showed that the MCF-7/A cells were sensitive to the effects of DPT. In contrast, with the resistance index of 754.5 and 38.94, respectively, PTX and Etoposide exerted decreased efficacy on the MCF-7/A cells.

3.5 DPT induced G2/M cell cycle arrest in both MCF-7/S and MCF-7/A cells

Generally, cell cycle progression is strongly associated with tubulin polymerization. Inhibition of tubulin polymerization has been implicated in G2/M cell cycle arrest in numerous cancer cell lines. We then compared the effect of DPT and PTX on the cell cycle progression of the MCF-7/S and MCF-7/A cells by flow cytometry. As depicted in Fig. 4B and 4D, treatment with DPT (5 and 10 nM) caused a remarkable accumulation in the G2/M phase in dose-dependent manners with a concomitant decrease in the G1 phase in both the MCF-7/S and MCF-7/A cells. DPT induced obvious G2/M arrest at 5 nM. The percentage of MCF-7/S and MCF-7/A cells in the G2/M phase was 14.94% and 32.32%, respectively. In stark contrast to DPT, although PTX exerted a similar efficacy on the MCF-7/S cells, no induction was observed on the MCF-7/A cells (Fig. 4A and 4C). These results indicated that DPT might be more active than PTX in the treatment of drug refractory tumors, especially those with resistance to PTX.

3.6 DPT destabilized microtubule assembly in a different mode from that of PTX

DMD Fast Forward. Published on March 9, 2018 as DOI: 10.1124/dmd.117.079442
This article has not been copyedited and formatted. The final version may differ from this version.

It has been reported that PTX can bind to the β-tubulin and stabilize microtubules. To determine the efficacy of DPT and PTX, we conducted the turbidity assay by recording the absorbance of the purified tubulin at 340 nM after incubation with PTX and DPT. The results indicated the anti-tubulin polymerization activities of DPT in a concentration-dependent manner as shown by the absence of the polymerized tubulin. In contrast, PTX resulted in a distinctive stabilization of microtubules as expected (Fig. 5).

3.7 Cellular and subcellular accumulation of DPT in MCF-7/A cells is similar to that in MCF-7/S cells

We monitored the intracellular and subcellular concentrations quantitatively by LC/MS/MS to further demonstrate the efficacy of DPT and PTX in the MCF-7/S and MCF-7/A cells and to explore the underlying mechanism. As seen in Fig. 6A, the intracellular retention of DPT in the MCF-7/A cells was higher than that in the MCF-7/S cells during the designated period. Intriguingly, the accumulation of PTX in the MCF-7/A cells was more than 5-fold lower than that in the MCF-7/S cells, which might be the major reason for PTX resistance in the MCF-7/A cells (Fig. 6B). Concurrently and sequentially, we also compared the intracellular accumulation of DPT and PTX in both of the cell lines at the designated time of 2 h (Fig. 6C), in line with the results above. As the cytosol acted as the target of DPT and PTX, we made further investigations into the subcellular distribution. The time-course analysis revealed the different subcellular distribution of DPT and PTX in both MCF-7/S and MCF-7/A cells (Fig. 6D, E, F). As shown in Fig. 6D, both DPT and PTX (89.9% and 92.4%, respectively) were primarily located in the cytosol, but they exerted distinctive retention differences in the MCF-7/S and MCF-7/A cells. These results indicated that the varied effect

DMD Fast Forward. Published on March 9, 2018 as DOI: 10.1124/dmd.117.079442
This article has not been copyedited and formatted. The final version may differ from this version.

of DPT and PTX might be due to different intracellular and subcellular accumulations.

Since P-gp governs the extrude of many anticancer drugs, the efflux assay was also conducted. Intriguingly, the retention curve of DPT in MCF-7/A cells was a little higher than that in MCF-7/S cells, while the retention of PTX in MCF-7/A cells was decreased to one in fifteen of that in MCF-7/S cells. P-gp inhibitor verapamil did not affect the efflux of DPT either in MCF-7/S or MCF-7/A cells. However, due to the efflux inhibition, the accumulation of PTX increased by two times in MCF-7/A cells when pretreated with verapamil (Fig. 6G, H). Also, PTX exerted higher efficacy in MCF-7/A cells with the Verapamil treatment (IC_{50}=188.78±26.34 nM) than PTX alone (IC_{50}=5011±920 nM), whereas DPT maintained its cytotoxicity in MCF-7/A cells with (IC_{50}=4.47±0.25 nM) or without Verapamil (4.64±0.25 nM) (Fig. 6I, J).

3.8 Effect of DPT on different efflux transporters *in vivo* and *in vitro*

We mined the current available data to further delineate the underlying molecular mechanism for DPT's better efficacy in the treatment of the MCF-7/A xenografts, and we explored the potential of DPT on different efflux transporters by determining the intracellular accumulation of the classic substrate for rapid screening. As expected, the established P-gp, BCRP (Breast Cancer Resistance Protein), and MRP2 (Multi-drug Resistance-associated Protein 2) inhibitor Verapamil (Zhang et al., 2010), KO143 (Matsson et al., 2009) and MK571 (Chen et al., 2017) exhibited a potent inhibitory effect on P-gp, BCRP, and MRP2, respectively, resulting in a palpable increase in the intracellular accumulation of the efflux transporter substrates Digoxin (DOX) (Zhang et al., 2010), SN-38 (Houghton et al., 2004), and CDCF (Chen et al., 2017). However, the retention of DPT did not shift in the absence

DMD Fast Forward. Published on March 9, 2018 as DOI: 10.1124/dmd.117.079442
This article has not been copyedited and formatted. The final version may differ from this version.

versus presence of the different inhibitors (Fig. 7A-C). Subsequently, we ascertained whether DPT could exert an effect on the intracellular accumulation of the substrates. Apparently, DPT exhibited no effect on the retention of the three substrates with various concentrations (Fig. 7D-F). Combing the results of the intracellular amounts above, P-gp, BCRP, and MRP2 might not mediate the transport of DPT

To further confirm that DPT was not the substrate of P-gp, we monitored the flux of DPT across WT-MDCK and MDR1/P-gp over-expressing MDR1-MDCK cell monolayers in the AP-BL and BL-AP directions in the absence or presence of Verapamil (Fig. 7G and 7H). WT-MDCK cells were applied as a negative control with a low expression of constitutive canine P-gp. Consistent with the results of the Caco-2 retention studies, the efflux ratio of DPT was approximately 1.0, which was less than the threshold of 2.0 for defining whether the drug acted as the substrate of P-gp or not, and did not change in the absence or presence of Verapamil. In contrast, Verapamil remarkably increased the transport of DGX in the AP-BL direction and decreased in the BL-AP direction, with the efflux ratio changing from 81.52 which was far more than 2.0 to 3.97. Thus, DPT was not the substrate of P-gp.

4. Discussion

The incidence of breast cancer and mortality have increased throughout the world (Althuis et al., 2005), and it remains the most common cancer in women (Murray et al., 2012). In recent years, more and more drugs explored in clinical trials have provided promising advances in breast cancer treatments. Microtubule-binding agents are among the efficacious chemotherapeutic drugs that are commonly used for the treatment of breast cancer. Although

anti-microtubule drugs, such as PTX and docetaxel, have been successfully applied in the clinic, drug resistance often occurred (Kavallaris, 2010) and acted as an obstacle for first-line chemotherapy. Augmented efflux transporters and diverse β-tubulin isotypes were involved in the development of drug resistance (Dumontet and Sikic, 1999). Thus, there is a pressing need to develop new microtubule inhibitors that can escape from the efflux of transporters related to MDR.

As a promising microtubule inhibitor candidate, DPT possesses various pharmacological activities, including anti-inflammatory (Jin et al., 2008), anti-viral (Gordaliza et al., 1994), anti-angiogenic (Wang et al., 2015a), and anti-tumor effects, among which anti-tumor attracted most attention. Previous studies have shown that DPT inhibits the proliferation of SGC-7901 cancer cells and induces G2/M cell cycle arrest (Wang et al., 2015b). Animal experiments revealed that DPT showed potent toxicity in lung cancer (Wu et al., 2013). Additionally, glioma growth could be inhibited by DPT *in vivo* and *in vitro*, which could be attributed to the upregulation of PARP-1 and AIF nuclear translocation (Ma et al., 2016). Although DPT induced apoptosis of the human BC mDA-MB-231 cell line *in vitro* (Benzina et al., 2015), little research has been conducted on the efficacy of DPT on the MCF-7 cell line. Whether DPT avoid MDR has yet to be investigated. In our study, Adriamycin-resistant MCF-7/A cells were used to explore the MDR influence of DPT. It is noteworthy that the cytotoxicity of DPT in drug-resistant MCF-7/A cells equals that in drug-sensitive MCF-7/S cells as indicated by IC_{50}, which is much better than the effect of PTX. In current studies, several lines of evidence indicated that DPT exhibited an inhibitory effect on the growth of various tumors. In a concentration-dependent manner, DPT exerted anti-tumor effects better

DMD Fast Forward. Published on March 9, 2018 as DOI: 10.1124/dmd.117.079442
This article has not been copyedited and formatted. The final version may differ from this version.

than Etoposide on H460 xenografts but with fewer side effects (Wu et al., 2013). Additionally, strong tumor inhibition properties were also observed on MDA-MB-231 human BC xenografts in the BALB/c nude mice model (Khaled et al., 2016). According to previous studies, we chose 12.5 mg/kg of DPT formulated as β-cyclodextrin inclusion complex (Zhu et al., 2010) as the target dose for intravenous injection to illuminate the *in vivo* antitumor effect of DPT with the MCF-7/S and MCF-7/A xenograft models. On the MCF-7/S xenograft models, DPT showed comparable inhibition effects to PTX as depicted in Fig. 2. Surprisingly, DPT maintained its tumor growth suppression of the MCF-7/A xenograft models, whereas PTX exerted a marginal inhibitory rate, suggesting that PTX had developed resistance. This was further evidenced by the histopathological examination of the tumors. Of particular interest, the concentration of DPT in the MCF-7/A xenografts was higher than that in the MCF-7/S xenografts, along with the plasma/tumor ratio. To our knowledge, this was the first time that the proliferation inhibition of DPT on MCF-7/S cells and related drug-resistant MCF-7/A cells *in vivo* and *in vitro* was proven.

Since DPT exerted a similar cytotoxicity on both of the drug-sensitive and drug-resistant xenograft models *in vivo*, further *in vitro* data confirmed the equal cytotoxicity of DPT on drug-sensitive and resistant MCF-7 cells with the indicated cell cycle assay. These results revealed that DPT might overcome multi-drug resistance in comparison with PTX. Although they are both microtubule-targeting agents, DPT may act in a different mode from PTX. Tubulin-targeting agents are generally classified into two groups: microtubule-stabilizing agents, such as paclitaxel, and microtubule-destabilizing agents, such as colchicine. PTX was investigated to reduce the purified tubulin subunits that are critical for polymerization into

microtubules (Weaver, 2014) and to shift the tubulin from its assembly equilibrium to its polymeric state (Prota et al., 2013). The results of the microtubule polymerization test confirmed the different binding modes of DPT and PTX. The manner in which DPT acts on microtubules may be the cause of its escape from the resistance transporters. Therefore, this discrepancy underscores the need to determine the underlying mechanism.

From the cellular pharmacokinetics perspective (Zhou et al., 2011), after penetrating the cell membrane, the anti-cancer drugs must bind to the intracellular target, thus exerting efficacy. Therefore, the intracellular distribution and disposition processes of the drugs acted as the determinants of their therapeutic effect (Krishan et al., 1997; Duvvuri and Krise, 2005). As reported, the weakened efficacy of PTX was ascribed to the efflux transporters, which not only restricted the distribution of the drug intracellularly, but they also reduced intracellular exposure (Argov et al., 2010). Herein, we established a novel LC/MS/MS method to compare the intracellular accumulation of PTX and DPT. From our results, the time-concentration curve demonstrated remarkable differences in the intracellular behavior of PTX between the MCF-7/S and MCF-7/A cells, whereas DPT exerted a similar retention in the two cell lines (Fig. 6). This is in line with our previous data revealing the discrepancy_involving the accumulation of DPT and PTX in the MCF-7/S and MCF-7/A xenografts. Support for this notion came from our findings that the subcellular distribution of DPT and PTX exhibited distinctive differences in the accumulation in different cellular organs, especially in cytosol. Based on the efflux assay, all the results indicated that the different behaviors of intracellular uptake, even subcellular disposition in drug-sensitive and drug-resistant cells, might determine their therapeutic efficacy (Xiong et al., 2010).

DMD Fast Forward. Published on March 9, 2018 as DOI: 10.1124/dmd.117.079442
This article has not been copyedited and formatted. The final version may differ from this version.

Then, Caco-2 cells and MDR1-MDCK cells were used to verify that DPT was not a substrate of these efflux transporters related to MDR. Due to the rich expression of the efflux transporters in the apical membrane, Caco-2 cell monolayers have been widely used to study drug intestinal absorption and the possible interaction with efflux transporters (Zhang et al., 2010). We provided ample evidence that DPT might not be the substrate of the three efflux transporters (P-gp, BCRP, and MRP2). In emerging studies, the MDR1-MDCK cell model has been used to screen P-gp substrates or inhibitors, expressed by apparent permeability (P_{app}). Herein, we found that the efflux ratio of DPT did not change with or without Verapamil, and it was less than the threshold for the definition of a P-gp substrate, which confirmed that DPT was not the substrate of P-gp. The findings may illustrate DPT's better efficacy in the treatment of MCF-7/A xenografts.

In consideration of all of the above, we have provided several lines of evidence that first illuminate that DPT exerted a proliferation inhibition effect on MCF-7/S and resistant MCF-7/A cells *in vitro* and *in vivo* in comparison with PTX. Moreover, we initially confirmed that DPT was not a substrate of the P-gp efflux pump and could overcome P-gp-mediated multi-drug resistance. Thus, DPT, as a new tubulin polymerization inhibitor, can be exploited as a promising agent for the treatment of multi-drug–resistant tumors.

Acknowledgments

We gratefully appreciated the help of all the staff, colleagues and students during the animal experiments. We showed our thanks to LetPub (www.letpub.com) for its linguistic assistance during the revision of this manuscript.

DMD Fast Forward. Published on March 9, 2018 as DOI: 10.1124/dmd.117.079442
This article has not been copyedited and formatted. The final version may differ from this version.

Authorship Contributions

Conceived the study: Fang Zhou, Haiping Hao

Participated in research design: Fang Zhou, Haiping Hao, Xiaojie Zang, Guangji Wang

Generated reagents or analytical tools: Fang Zhou, Xiaojie Zang, Qingyun Cai, Baojin Wu, Xiong Zhu

Conducted experiments: Fang Zhou, Haiping Hao, Xiaojie Zang, Qingyun Cai, Jingwei Zhang and Qianying Chen

Performed data analysis: Fang Zhou, Xiaojie Zang, Qingyun Cai, Xiao Zheng, Qianying Chen, Baojin Wu

Wrote or contributed to the writing of the manuscript: Fang Zhou, Haiping Hao, Xiaojie Zang, Guangji Wang

References

Althuis, M.D., Dozier, J.M., Anderson, W.F., Devesa, S.S., and Brinton, L.A. (2005). Global trends in breast cancer incidence and mortality 1973-1997. *Int. J. Epidemiol* 34(2)**,** 405-412. doi: 10.1093/ije/dyh414.

Argov, M., Bod, T., Batra, S., and Margalit, R. (2010). Novel steroid carbamates reverse multidrug-resistance in cancer therapy and show linkage among efficacy, loci of drug action and P-glycoprotein's cellular localization. *Eur. J. Pharm Sci* 41(1)**,** 53-59. doi: 10.1016/j.ejps.2010.05.012.

Benzina, S., Harquail, J., Jean, S., Beauregard, A.P., Colquhoun, C.D., and Carroll, M., et al. (2015). Deoxypodophyllotoxin isolated from Juniperus communis induces apoptosis in breast cancer cells. *Anticancer Agents Med. Chem* 15(1)**,** 79-88.

Bliss, C. I. (1939). The toxicity of poisons applied jointly. *Annals of Applied Biology*, 26(3), 585–615.

Cao, B., Aa, J., Wang, G., Wu, X., Liu, L., and Li, M., et al. (2011). GC-TOFMS analysis of metabolites in adherent MDCK cells and a novel strategy for identifying intracellular metabolic markers for use as cell amount indicators in data normalization. *Anal. Bioana.l Chem* 400(9)**,** 2983-2993. doi: 10.1007/s00216-011-4981-8.

Chen, Q., Chen, H., Wang, W., Liu, J., Liu, W., and Ping, N., et al. (2017). Glycyrrhetic acid, but not glycyrrhizic acid, strengthened entecavir activity by promoting its subcellular distribution in the liver via, efflux inhibition.*European Journal of Pharmaceutical Sciences Official Journal of the European Federation for Pharmaceutical Sciences*, 106, 313.

Chen, Y., Zhao, K., Liu, F., Xie, Q., Zhong, Z., and Miao, M., et al. (2016). Prediction of Deoxypodophyllotoxin Disposition in Mouse, Rat, Monkey, and Dog by Physiologically Based Pharmacokinetic Model and the Extrapolation to Human. *Front. Pharmacol* 7**,** 488. doi: 10.3389/fphar.2016.00488.

Dumontet, C., and Jordan, M.A. (2010). Microtubule-binding agents: a dynamic field of cancer therapeutics. *Nat Rev. Drug. Discov* 9(10)**,** 790-803. doi: 10.1038/nrd3253.

Dumontet, C., and Sikic, B.I. (1999). Mechanisms of action of and resistance to antitubulin agents: microtubule dynamics, drug transport, and cell death. *J. Clin. Oncol* 17(3)**,** 1061-1070. doi: 10.1200/jco.1999.17.3.1061.

Duvvuri, M., and Krise, J.P. (2005). Intracellular drug sequestration events associated with the emergence of multidrug resistance: a mechanistic review. *Front. Biosci* 10**,** 1499-1509.

Gordaliza, M., Castro, M.A., Garcia-Gravalos, M.D., Ruiz, P., Miguel del Corral, J.M., and San Feliciano, A. (1994). Antineoplastic and antiviral activities of podophyllotoxin related lignans. *Arch. Pharm (Weinheim)* 327(3)**,** 175-179.

Gottesman, M.M. (1993). How Cancer-Cells Evade Chemotherapy - 16th Richard-And-Hinda-Rosenthal-Foundation Award Lecture. *Cancer Research* 53(4)**,** 747-754.

Houghton, P. J., Germain, G. S., Harwood, F. C., Schuetz, J. D., Stewart, C. F., and Buchdunger, E., et al. (2004). Imatinib mesylate is a potent inhibitor of the abcg2 (bcrp) transporter and reverses resistance to topotecan and sn-38 in vitro. *Cancer Research*, 64(7), 2333.

Howard, J., and Hyman, A.A. (2003). Dynamics and mechanics of the microtubule plus end.

Nature 422(6933)**,** 753-758. doi: 10.1038/nature01600.

Jin, M., Moon, T.C., Quan, Z., Lee, E., Kim, Y.K., Yang, J.H., et al. (2008). The naturally occurring flavolignan, deoxypodophyllotoxin, inhibits lipopolysaccharide-induced iNOS expression through the NF-kappaB activation in RAW264.7 macrophage cells. *Biol. Pharm. Bull* 31(7)**,** 1312-1315.

Kavallaris, M. (2010). Microtubules and resistance to tubulin-binding agents. *Nat. Rev. Cancer* 10(3)**,** 194-204. doi: 10.1038/nrc2803.

Khaled, M., Belaaloui, G., Jiang, Z.Z., Zhu, X., and Zhang, L.Y. (2016). Antitumor effect of Deoxypodophyllotoxin on human breast cancer xenograft transplanted in BALB/c nude mice model. *J. Infect. Chemother* 22(10)**,** 692-696. doi: 10.1016/j.jiac.2016.07.017.

Khaled, M., Jiang, Z.Z., and Zhang, L.Y. (2013). Deoxypodophyllotoxin: a promising therapeutic agent from herbal medicine. *J. Ethnopharmacol* 149(1)**,** 24-34. doi: 10.1016/j.jep.2013.06.021.

Kim, K.Y., Cho, H.J., Yu, S.N., Kim, S.H., Yu, H.S., Park, and Y.M., et al. (2013). Interplay of reactive oxygen species, intracellular Ca2+ and mitochondrial homeostasis in the apoptosis of prostate cancer cells by deoxypodophyllotoxin. *J. Cell. Biochem* 114(5)**,** 1124-1134. doi: 10.1002/jcb.24455.

Kodama, N., Iwao, T., Katano, T., Ohta, K., Yuasa, H., and Matsunaga, T. (2016). Characteristic analysis of intestinal transport in enterocyte-like cells differentiated from human induced pluripotent stem cells. *Drug Metab. Dispos*, 44(10). doi: 10.1124/dmd.116.069336.

Krishan, A., Fitz, C.M., and Andritsch, I. (1997). Drug retention, efflux, and resistance in tumor cells. *Cytometry* 29(4)**,** 279-285.

Liu, W.Y., Zhang, J.W., Yao, X.Q., Jiang, C., He, J.C., and Ni, P., et al. (2017). Shenmai injection enhances the cytotoxicity of chemotherapeutic drugs against colorectal cancers via improving their subcellular distribution. *Acta. Pharmacol. Sin* 38(2)**,** 264-276. doi: 10.1038/aps.2016.99.

Lu, M., Zhou, F., Hao, K., Liu, J., Chen, Q., and Ni, P., et al. (2015). Alternation of adriamycin penetration kinetics in mcf-7 cells from 2d to 3d culture based on p-gp expression through the chk2/p53/nf-κb pathway. *Biochemical Pharmacology*, 93(2), 210. doi: 10.1016/j.bcp.2014.11.010.

Ma, D., Lu, B., Feng, C., Wang, C., Wang, Y., and Luo, T., et al. (2016). Deoxypodophyllotoxin triggers parthanatos in glioma cells via induction of excessive ROS. *Cancer Lett* 371(2)**,** 194-204. doi: 10.1016/j.canlet.2015.11.044.

Matsson, P., Pedersen, J. M., Norinder, U., Bergström, C. A. S., and Artursson, P. (2009). Identification of novel specific and general inhibitors of the three major human atp-binding cassette transporters p-gp, bcrp and mrp2 among registered drugs. *Pharmaceutical Research*, 26(8), 1816-1831.

Murray, S., Briasoulis, E., Linardou, H., Bafaloukos, D., and Papadimitriou, C. (2012). Taxane resistance in breast cancer: mechanisms, predictive biomarkers and circumvention strategies. *Cancer Treat. Rev* 38(7)**,** 890-903. doi: 10.1016/j.ctrv.2012.02.011.

Poirier, A., Cascais, A. C., Bader, U., Portmann, R., Brun, M. E., Walter, I., et al. (2014).

Calibration of in vitro multidrug resistance protein 1 substrate and inhibition assays as a basis to support the prediction of clinically relevant interactions in vivo. *Drug Metab. Dispos*, 42(9), 1411-1422. doi: 10.1124/dmd.114.057943.

Prota, A.E., Bargsten, K., Zurwerra, D., Field, J.J., Diaz, J.F., Altmann, K.H., et al. (2013). Molecular mechanism of action of microtubule-stabilizing anticancer agents. *Science* 339(6119)**,** 587-590. doi: 10.1126/science.1230582.

Ranaldi, G., Seneci, P., Guba, W., Islam, K., and Sambuy, Y. (1996). Transport of the antibacterial agent oxazolidin-2-one and derivatives across intestinal (caco-2) and renal (mdck) epithelial cell lines. *Antimicrobial Agents and Chemotherapy*, 40(3), 652.

Shin, S.Y., Yong, Y., Kim, C.G., Lee, Y.H., and Lim, Y. (2010). Deoxypodophyllotoxin induces G2/M cell cycle arrest and apoptosis in HeLa cells. *Cancer Lett* 287(2)**,** 231-239. doi: 10.1016/j.canlet.2009.06.019.

Tulkens, P.M. (1990). Intracellular pharmacokinetics and localization of antibiotics as predictors of their efficacy against intraphagocytic infections. *Scand J. Infect. Dis. Suppl* 74**,** 209-217.

Wang, Y., Wang, B., Guerram, M., Sun, L., Shi, W., Tian, C., et al. (2015a). Deoxypodophyllotoxin suppresses tumor vasculature in HUVECs by promoting cytoskeleton remodeling through LKB1-AMPK dependent Rho A activatio. *Oncotarget* 6(30)**,** 29497-29512. doi: 10.18632/oncotarget.4985.

Wang, Y.R., Xu, Y., Jiang, Z.Z., Guerram, M., Wang, B., Zhu, X., et al. (2015b). Deoxypodophyllotoxin induces G2/M cell cycle arrest and apoptosis in SGC-7901 cells and inhibits tumor growth in vivo. *Molecules* 20(1)**,** 1661-1675. doi:

10.3390/molecules20011661.

Weaver, B.A. (2014). How Taxol/paclitaxel kills cancer cells. *Mol. Biol. Cell* 25(18), 2677-2681. doi: 10.1091/mbc.E14-04-0916.

Wu, M., Jiang, Z., Duan, H., Sun, L., Zhang, S., Chen, M., et al. (2013). Deoxypodophyllotoxin triggers necroptosis in human non-small cell lung cancer NCI-H460 cells. *Biomed. Pharmacother* 67(8), 701-706. doi: 10.1016/j.biopha.2013.06.002.

Xiong, X.B., Ma, Z., Lai, R., and Lavasanifar, A. (2010). The therapeutic response to multifunctional polymeric nano-conjugates in the targeted cellular and subcellular delivery of doxorubicin. *Biomaterials* 31(4), 757-768. doi: 10.1016/j.biomaterials.2009.09.080.

Yang Y., Chen Y., Zhong Z., Zhang J., Li F, Jia L., et al. (2014). Validated LC–MS/MS assay for quantitative determination of deoxypodophyllotoxin in rat plasma and its application in pharmacokinetic study. *Journal of Pharmaceutical and Biomedical Analysis* 88, 410-415. doi: 10.1016/j.jpba.2013.09.027.

Zhang, J., Zhou, F., Wu, X., Gu, Y., Ai, H., Zheng, Y., et al. (2010). 20(S)-ginsenoside Rh2 noncompetitively inhibits P-glycoprotein in vitro and in vivo: a case for herb-drug interactions. *Drug Metab. Dispos* 38(12), 2179-2187. doi: 10.1124/dmd.110.034793.

Zhang, J., Zhou, F., Wu, X., Zhang, X., Chen, Y., Zha, B.S., et al. (2012). Cellular pharmacokinetic mechanisms of adriamycin resistance and its modulation by 20(S)-ginsenoside Rh2 in MCF-7/Adr cells. *Br. J. Pharmacol* 165(1), 120-134. doi: 10.1111/j.1476-5381.2011.01505.x.

Zhou, F., Zhang, J., Li, P., Niu, F., Wu, X., Wang, G., et al. (2011). Toward a new age of cellular pharmacokinetics in drug discovery. *Drug Metab. Rev* 43(3), 335-345. doi: 10.3109/03602532.2011.560607.

Zhu, X., Wu, B.J., Luo, H.W., Tao, L., Zhao, Q., Guo, Q.L., et al. (2010). Preparation of solid inclusion complex of deoxypodophyllotoxin - SBE-β-CD and its antitumor activity. *Journal of China Pharmaceutical University* 41(5), 447-450.

DMD Fast Forward. Published on March 9, 2018 as DOI: 10.1124/dmd.117.079442
This article has not been copyedited and formatted. The final version may differ from this version.

Footnotes

The work was supported by China National Nature Science Foundation [Grants 81573496, 81530098]; Jiangsu Province Key Lab of Drug Metabolism and Pharmacokinetics Projects [Grant BM2012012]; Jiangsu Province Nature Science Foundation [Grant BK20160076]; China "Creation of New Drugs" Key Technology Projects [Grant 2015ZX09501001]; the Foundation for Innovative Research Groups of the National Natural Science Foundation of China [Grant 81421005]; the Project Program of State Key Laboratory of Natural Medicines, China Pharmaceutical University [Grant SKLNMZZCX201608].

X.Z. and G.W. contributed equally to this work.

Legends for Figures

Figure 1 DPT inhibited the growth of MCF-7/S and MCF-7/A tumors in nude mice. Representative photos of the xenografts excised from MCF-7/S (A) and MCF-7/A (B) xenograft models are presented. The average weight of the xenografts excised from MCF-7/S (C) and MCF-7/A (D) xenograft models is shown. The average volume of the MCF-7/S (E) and MCF-7/A (F) xenografts in nude mice were both inhibited by DPT, with dosing schedules following every 3 days. On the contrary, PTX exerted no effects on the growth of the MCF-7/A xenografts, with dosing schedules following every 3 days. A vernier caliper was used to measure the tumor diameter serially, followed by the calculation of the relative tumor volume using the equations expressed in the Methods section. The percentage of tumor volume growth of the MCF-7/S (G) and MCF-7/A (H) xenograft models was expressed under the treatment of DPT and PTX. Data are expressed as mean± SD. *$P < 0.05$, **$P < 0.01$, ***$P<0.001$, ****$P<0.0001$ versus control.

Figure 2 DPT supplementation in the MCF-7/S (A) and MCF-7/A (B) xenograft models increased nuclear pleomorphsim and necrosis. Tumors excised from the xenograft models were fixed with formalin and sectioned for hematoxylin-eosin (H&E) staining with the magnification of ×100.

Figure 3 Biodistribution of DPT and PTX in the MCF-7/S and MCF-7/A xenograft models. (A) Concentration-time curve of DPT and PTX in the plasma of the MCF-7/S and MCF-7/A xenograft mice. (B) The concentration of DPT and PTX in tumors excised from MCF-7/S and MCF-7/A xenograft mice. (C) The plasma/tumor ratio of DPT and PTX in the MCF-7/S and MCF-7/A xenograft mice; it was calculated by the average concentration of DPT or PTX in

the plasma versus that in the tumor at the designated time (45 min after injection). (D) Drug biodistribution of DPT and PTX in non-malignant tissues from the heart, liver, spleen, lung and kidney of the MCF-7/S and MCF-7/A xenograft mice. Data are presented as mean ± SD. *P < 0.05, **P < 0.01, ***P<0.001, ****P<0.0001 versus control.

Figure 4 Compared with PTX, DPT induced G2/M cycle arrest in the MCF-7/S and MCF-7/A cells. (A, B) PTX and DPT caused G2/M phase arrest in the MCF-7/S cell at concentrations of 1, 5, and 10 nM for 12 h. (C) PTX did not induce cell cycle progression in the MCF-7/A cells. (D) DPT arrested the MCF-7/A cells at the G2/M phase at the specified concentrations of 1, 5, and 10 nM. Histograms represent the percentage of cell cycle distribution at the G2/M phase. Data are presented as mean ± SD of three independent experiments. *P < 0.05, **P < 0.01 versus control (0 nM).

Figure 5 Effect of DPT and PTX on tubulin polymerization. The efficacy of DPT (1, 2, 5, 10, and 20 μM) and PTX (10 μM) on tubulin polymerization was evaluated by turbidity changes recorded at the wavelength of 340 nm. The experiment was repeated three times. Data from the representative experiment are shown.

Figure 6 Time-course analysis of intracellular and subcellular accumulation of DPT and PTX in the MCF-7/S and MCF-7/A cells. (A, B) Intracellular retention of DPT and PTX in the MCF-7/S and MCF-7/A cells. Cells were incubated with 5 μM DPT and PTX for 15, 30, 60, and 120 min. (C) Area under the curve of the intracellular accumulation of DPT and PTX in the MCF-7/S and MCF-7/A cells at the designated time of 2 h. (D, E, F) Time-course analysis and Area under the curve of subcellular accumulation of DPT and PTX in the MCF-7/S and MCF-7/A cells. Cells were treated with 1 μM DPT and PTX for 15, 30, 45min, 1 and 2 h. (G,

H) Intracellular retention of DPT and PTX in the MCF-7/S and MCF-7/A cells with or without Verapamil. The cells were incubated with 5 μM DPT and PTX for 2 h, and then the retention of DPT or PTX within cells was monitored with or without Verapamil 0, 15, 30 60 and 120 min later. (I, J) Cell viability of DPT and PTX in MCF-7/S and MCF-7/A cells with or without Verapamil. Results are expressed as mean ± SD of three independent experiments. *P < 0.05, **P < 0.01, ***P<0.001, ****P<0.0001 versus control.

Figure 7 Effect of DPT on different efflux transporters *in vivo* and *in vitro*. (A-C) The accumulation of DPT in Caco-2 cells when treated with different efflux transporter inhibitors. Cells were pre-incubated with the inhibitors for 1 h followed by another 2 h of incubation in the presence of DPT. The inhibitors investigated (left to right) were Verapamil (20 μM), MK571 (10 μM), and KO143 (5 μM). DGX (5 μM), CDCF (10 μM), and SN-38 (10 μM) were used as the positive controls. (D-F) The retention of different substrates of the efflux transporters after DPT treatment with different concentrations. Cells were pre-incubated with DPT for 1 h followed by another 2 h of incubation in the presence of DGX, CDCF, and SN-38. (G, H) Effect of DPT on the transport of P-gp substrates across the WT-MDCK and MDR1-MDCK cell monolayers. DPT (0.5 and 1 μM) was loaded on either the AP or BL side and incubated for 2 h. DGX was treated as a P-gp substrate control. Verapamil was used as a P-gp inhibitor control. Data are presented as mean ± SD. *P < 0.05, **P < 0.01, ***P<0.001, ****P<0.0001 versus control.

DMD Fast Forward. Published on March 9, 2018 as DOI: 10.1124/dmd.117.079442
This article has not been copyedited and formatted. The final version may differ from this version.

Table 1 IC_{50}[a] values of DPT, PTX and Etoposide in MCF-7/S and MCF-7/A cells

	MCF-7/S IC_{50} (nM)	MCF-7/A IC_{50} (nM)	RI[b] (Resistance index)
DPT	10.61±1.09	5.86±0.30	0.552
PTX	7.005±0.445	5285±1095	754.5
Etoposide	17355±2695	675780±10450	38.94

a. Drug concentration required to inhibit cancer cell proliferation by 50%. Data are expressed as the mean ± SD from the dose-response curves of three independent experiments.

b. Resistance index: (IC_{50} of MCF-7/A cell) / (IC_{50} of MCF-7/S cell).

DMD Fast Forward. Published on March 9, 2018 as DOI: 10.1124/dmd.117.079442
This article has not been copyedited and formatted. The final version may differ from this version.

Figures

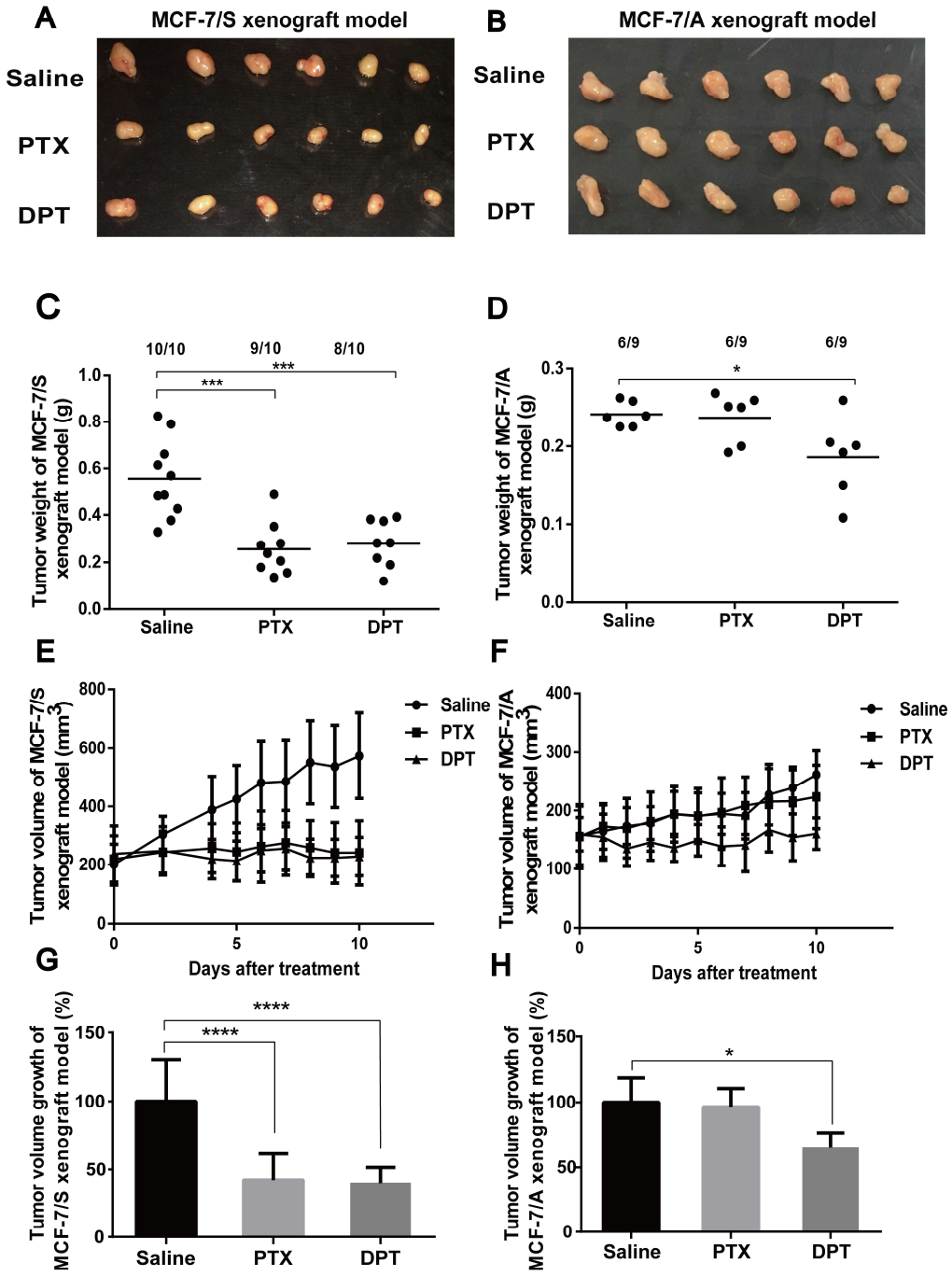

Figure1

DMD Fast Forward. Published on March 9, 2018 as DOI: 10.1124/dmd.117.079442
This article has not been copyedited and formatted. The final version may differ from this version.

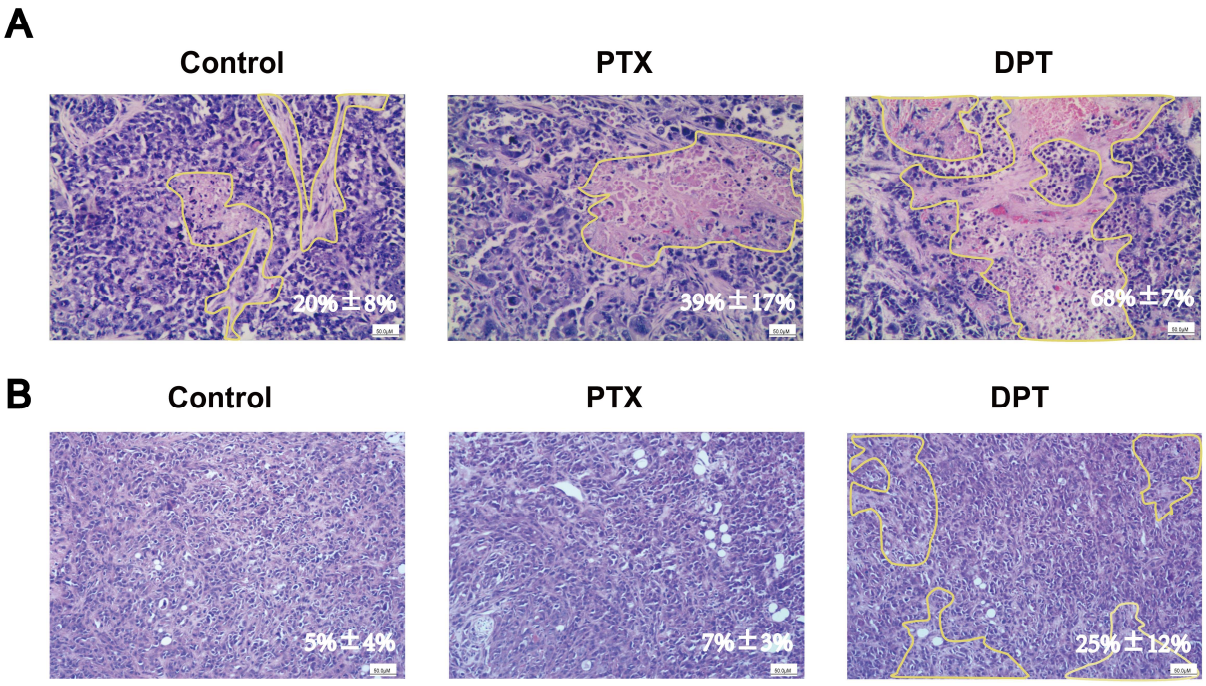

Figure2

DMD Fast Forward. Published on March 9, 2018 as DOI: 10.1124/dmd.117.079442
This article has not been copyedited and formatted. The final version may differ from this version.

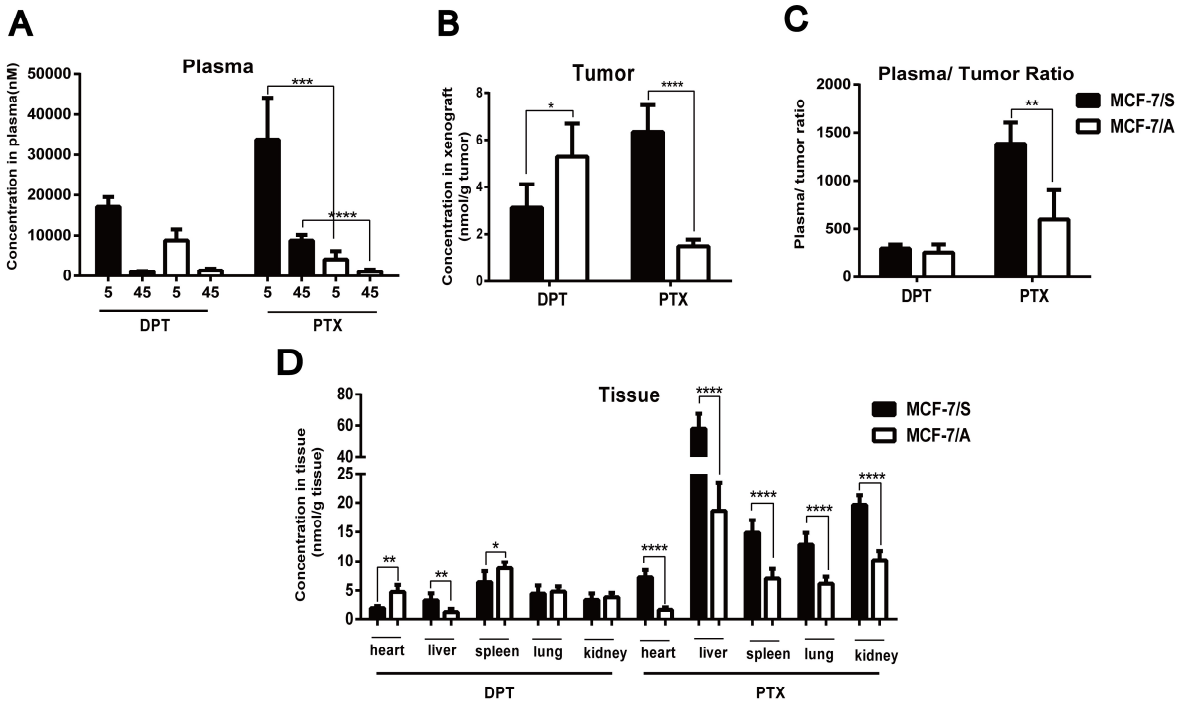

Figure3

DMD Fast Forward. Published on March 9, 2018 as DOI: 10.1124/dmd.117.079442
This article has not been copyedited and formatted. The final version may differ from this version.

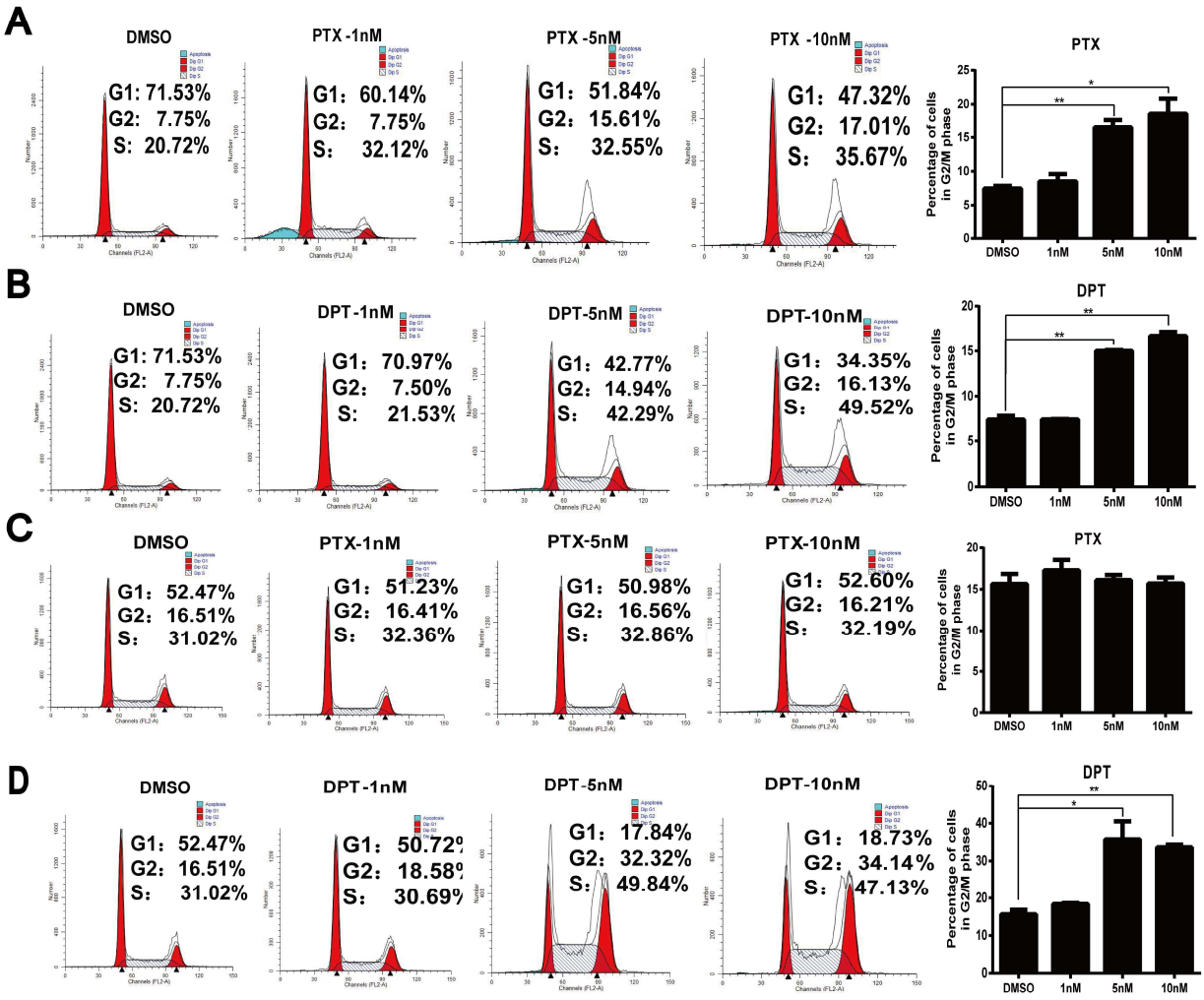

Figure4

DMD Fast Forward. Published on March 9, 2018 as DOI: 10.1124/dmd.117.079442
This article has not been copyedited and formatted. The final version may differ from this version.

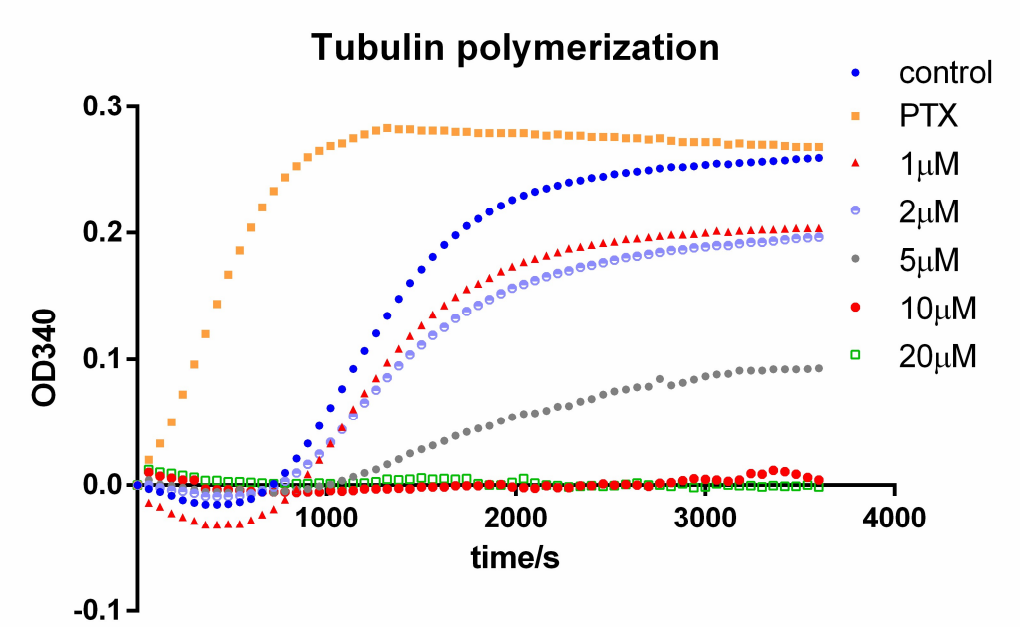

Figure5

DMD Fast Forward. Published on March 9, 2018 as DOI: 10.1124/dmd.117.079442
This article has not been copyedited and formatted. The final version may differ from this version.

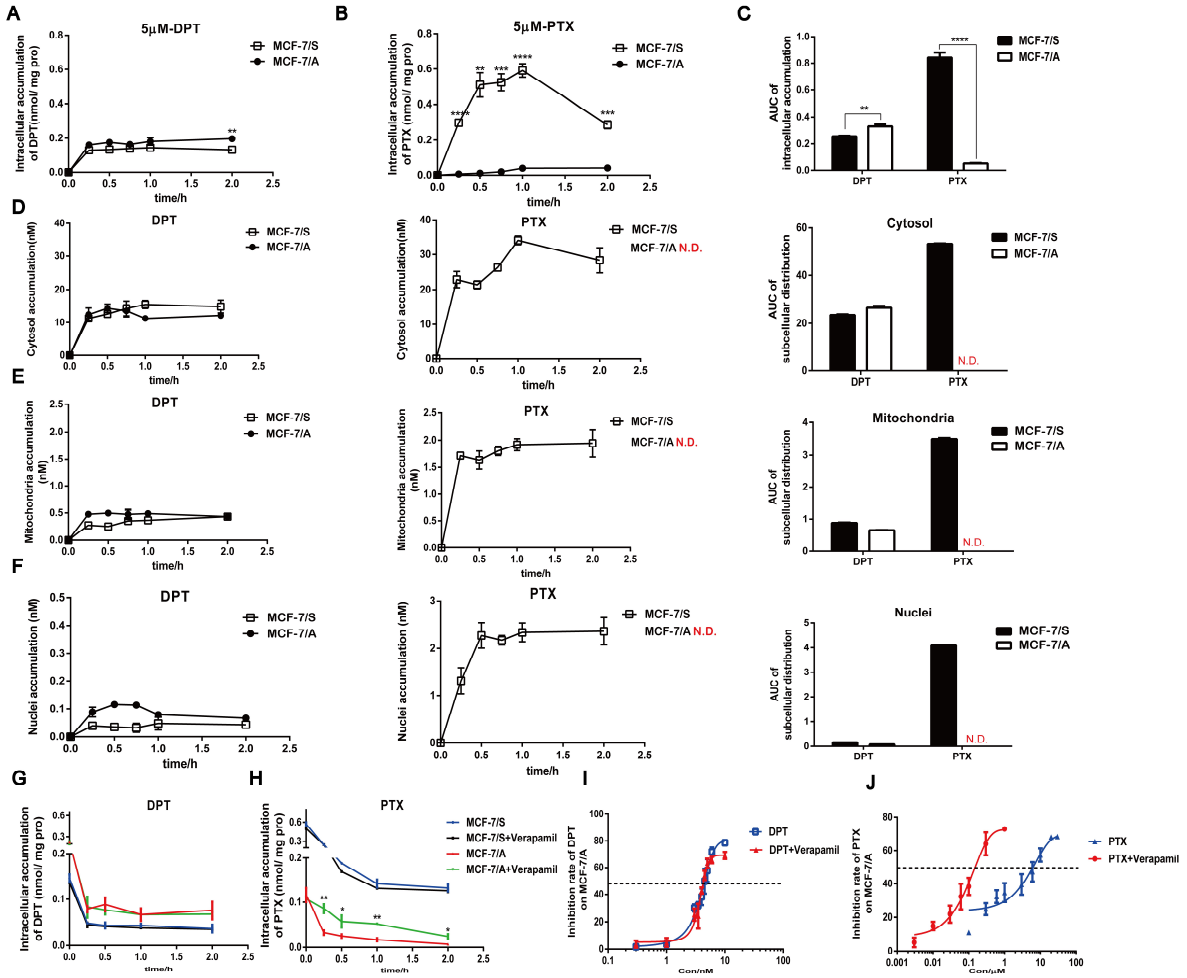

Figure6

DMD Fast Forward. Published on March 9, 2018 as DOI: 10.1124/dmd.117.079442
This article has not been copyedited and formatted. The final version may differ from this version.

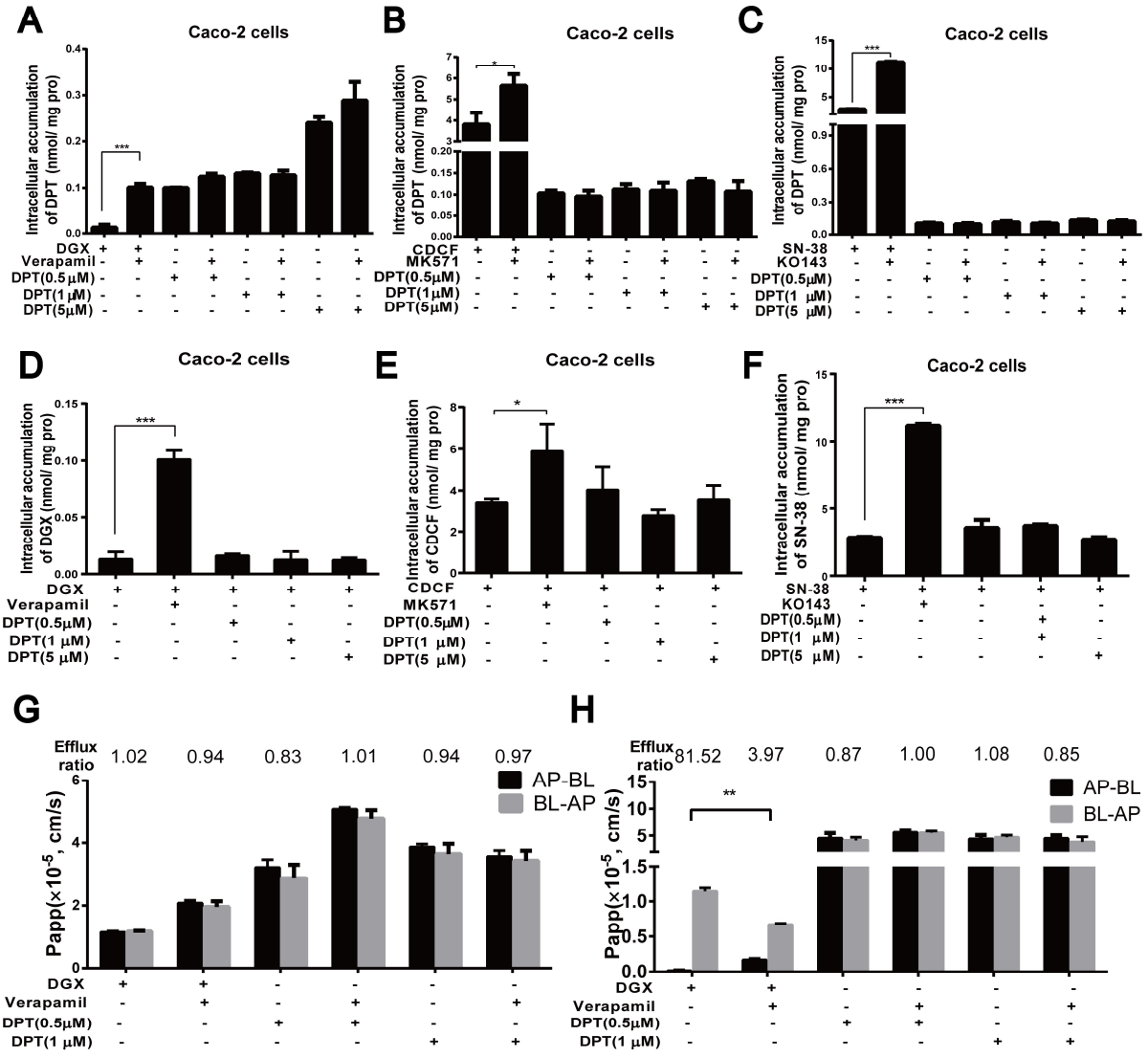

Figure7

Supplementary Data

A Promising Microtubule Inhibitor Deoxypodophyllotoxin Exhibits Better Efficacy to Multi-Drug Resistant Breast Cancer than Paclitaxel via Avoiding Efflux Transport

Xiaojie Zang, Guangji Wang, Qingyun Cai, Xiao Zheng, Jingwei Zhang, Qianying Chen, Baojin Wu, Xiong Zhu, Haiping Hao and Fang Zhou

Key Laboratory of Drug Metabolism and Pharmacokinetics, State Key Laboratory of Natural Medicines, China Pharmaceutical University, Nanjing, China (X.Z., G.W., Q.C., X.Z., J.Z., Q.C., H.H., F.Z.)

Medical and Chemical Institute, China Pharmaceutical University, Nanjing, China (B.W., X.Zhu.)

Drug metabolism and disposition

1. Linearity
   The standard curve exhibited a good linear relationship over the concentration range of 0.5-1000 ng/mL with a regression coefficient (r^2=0.9992 ± 0.0003).

2. Recovery and matrix effect
   Across the 5 independent experiments, the mean recovery of DPT ranged from 94.13% to 104.76% over the three concentrations. The precision was < 5.59%, which proved the reproducibility and consistency of the extraction method. Due to the matrix effect ranging from 98.27% to 102.29% and the precision < 5.85%, the suppression or enhancement could be neglected under the current conditions.

3. Precision and accuracy

   The intra- and inter-day precision and accuracy values for 5 replicates of QC samples at three nominated concentrations were shown in Table S1, which strongly supported the accuracy, reliability and reproducibility of the method.

Table S1 Intra- and inter-day precision and accuracy for DPT (n=5)

	Intra-day			Inter-day		
Nominal concentration (ng/ml)	Measured concentration (mean±SD, ng/ml)	Accuracy (RE, %)	Precision (RSD, %)	Measured concentration (mean±SD, ng/ml)	Accuracy (RE, %)	Precision (RSD, %)
1	1.00±0.06	0.00	6.00	1.00±0.09	0.01	8.60
20	21.14±0.69	5.70	3.26	20.87±0.70	4.37	3.34
1000	963.80±20.14	-3.62	2.09	960.93±28.75	-3.91	2.99

4. Stability

The stability of DPT was investigated under different conditions and was shown in Table S2, thus indicating that the samples were all stable under three freeze-thaw cycles, at -80 ˚C for 14 days and at room temperature for 24 h and under post-preparation in an autosampler tray (4 ˚C) for 24 h.

Table S2 Stability of DPT under different conditions at three QC levels (n=5)

Storage conditions	Nominal concentration (ng/ml)	Measured concentration (mean± SD)	Accuracy (RE, %)	Precision (RSD, %)
Three freeze-thaw cycles	1	0.98±0.06	-2.22	6.32
	20	20.40±0.93	2	4.55
	1000	983.60±18.83	-1.64	1.91
Frozen (-80˚C) for 14 days	1	0.85±0.08	-14.96	9.42
	20	20.20±0.71	1	3.53
	1000	961.80±39.76	-3.82	4.13
Room temperature for 24h	1	1.00±0.06	0.26	5.72
	20	21.18±0.32	5.9	1.51
	1000	963.40±45.91	-3.66	4.77
Post-preparation (4 ˚C) for 24h	1	1.03±0.10	2.56	9.72
	20	20.68±0.51	3.4	2.48
	1000	946.40±35.51	-5.36	3.75

5. Recovery and matrix effect

Table S3 Recovery and matrix effect of DPT in mitochondria (n=5)

Analytes	Spiked concentration (ng/mL)	Recovery (mean±SD%)	RSD(%)	Matrix effect (mean±SD%)	RSD(%)
DPT	1.00	100.86%±1.39%	1.38%	106.19%±3.16%	2.98%
	20.00	104.20%±5.06%	4.85%	98.74%±6.49%	6.57%
	1000.00	99.66%±5.90%	5.92%	97.08%±3.26%	3.36%

Table S4 Recovery and matrix effect of DPT in nuclei (n=5)

Analytes	Spiked concentration (ng/mL)	Recovery (mean±SD%)	RSD(%)	Matrix effect (mean±SD%)	RSD(%)
DPT	1.00	97.67%±7.13%	7.30%	106.16%±4.92%	4.63%
	20.00	103.91%±4.52%	4.35%	94.25%±6.53%	6.93%
	1000.00	99.85%±2.45%	2.45%	94.85%±4.46%	4.71%

Table S5 Recovery and matrix effect of DPT in cytosol (n=5)

Analytes	Spiked concentration (ng/mL)	Recovery (mean±SD%)	RSD(%)	Matrix effect (mean±SD%)	RSD(%)
DPT	1.00	95.13%±1.50%	1.57%	110.73%±3.65%	3.30%
	20.00	101.31%±5.69%	5.61%	101.64%±4.71%	4.64%
	1000.00	102.79%±7.02%	6.83%	106.80%±4.72%	4.42%

Table S6 Recovery and matrix effect of DPT in blood (n=5)

Analytes	Spiked concentration (ng/mL)	Recovery (mean±SD%)	RSD(%)	Matrix effect (mean±SD%)	RSD(%)
DPT	15.60	102.70%±5.17%	5.03	92.55%±4.92%	5.32
	125.00	107.72±4.68%	4.35	97.83%±7.21%	7.36
	500.00	96.75%±5.61%	5.80	98.88%±6.75%	6.82

Table S7 Recovery and matrix effect of DPT in liver (n=5)

Analytes	Spiked concentration (ng/mL)	Recovery (mean±SD%)	RSD(%)	Matrix effect (mean±SD%)	RSD(%)
DPT	15.47	100.54%±3.05%	3.54	97.22%±5.01%	5.15
	123.75	91.98%±2.95%	3.21	82.65±0.78%	0.94
	792.00	93.48%±3.42%	3.65	100.43%±2.74%	2.73

6. Quality control

Table S8 Quality control of DPT in heart, spleen, lung, kidney and tumor (n=5)

Analytes	Spiked concentration (ng/mL)	Heart		Spleen		Lung		Kidney		Tumor	
		Measured concentration (mean±SD%)	RE(%)	Measured concentration (mean±SD%)	RE(%)	Measured concentration (mean±SD%)	RE(%)	Measured concentration (mean±SD%)	RE(%)	Measured concentration (mean±SD%)	RE(%)
DPT	15.47	16.75±0.09	8.27	16.68±1.01	7.79	16.41±0.33	6.08	15.95±0.83	3.10	14.33±0.30	-7.37
	123.75	127.89±11.65	3.34	119.02±4.74	-3.82	131.04±6.25	5.89	127.65±4.99	3.15	130.36±3.55	5.34
	792.00	737.87±8.74	-6.83	778.74±0.28	-1.67	777.30±6.31	-1.86	1749.63±18.04	-5.35	746.87±10.49	-5.70